ADVANCED FUNCTIONAL MATERIALS

DOI: 10.1002/adfm.200500855

Enhancement of Modulus, Strength, and Toughness in Poly(methyl methacrylate)-Based Composites by the Incorporation of Poly(methyl methacrylate)-Functionalized Nanotubes**

By *David Blond*, *Valerie Barron*, *Manuel Ruether*, *Kevin P. Ryan*, *Valeria Nicolosi*, *Werner J. Blau*, and *Jonathan N. Coleman**

Poly(methyl methacrylate) (PMMA)-functionalized multiwalled carbon nanotubes are prepared by in situ polymerization. Infrared absorbance studies reveal covalent bonding between polymer strands and the nanotubes. These treated nanotubes are blended with pure PMMA in solution before drop-casting to form composite films. Increases in Young's modulus, breaking strength, ultimate tensile strength, and toughness of ×1.9, ×4.7, ×4.6, and ×13.7, respectively, are observed on the addition of less than 0.5 wt % of nanotubes. Effective reinforcement is only observed up to a nanotube content of approximately 0.1 vol %. Above this volume fraction, all mechanical parameters tend to fall off, probably due to nanotube aggregation. In addition, scanning electron microscopy (SEM) studies of composite fracture surfaces show a polymer layer coating the nanotubes after film breakage. The fact that the polymer and not the interface fails suggests that functionalization results in an extremely high polymer/nanotube interfacial shear strength.

1. Introduction

Since their discovery in 1991[1] carbon nanotubes (CNTs) have generated a great deal of interest owing to their unique physical properties, such as large aspect ratio, excellent current-carrying capability,[2] and high thermal conductivity.[3] They are suitable for a wide range of applications including electrochemical, field-emission, and electronic devices.[4] However, perhaps the most promising potential applications are those associated with their mechanical properties. For example, nanotubes' Young's moduli can reach 1 TPa,[5] while their strength has been measured at up to 63 GPa,[6] which is an order of magnitude stronger than high-strength carbon fibers.[7] This has allowed the fabrication of materials such as supertough polymer–nanotube composite fibers.[8] Recently, Coleman et al. fabricated composites based on poly(vinyl alcohol) demonstrating[9] an increase of ×3.7 in Young's modulus and ×3.9 in strength by adding less than 1 wt % of CNTs. In this case, the increase was intimately related to the nucleation of polymer crystallinity by the nanotubes. The resulting crystalline interfacial region plays a dual role. Because of its inherent strength and stiffness, it acts as a reinforcing agent in its own right. More importantly, it is thought that crystalline interfacial regions result in better stress transfer to nanotubes compared to amorphous regions.[10,11] Nevertheless, this method is not suitable for most types of polymer because of their inherently amorphous structure. As such, some method of interfacial engineering is required to maximize stress transfer in amorphous polymer matrices.

Several methods have been reported to produce amorphous polymer–nanotube composites with good dispersion and good stress transfer between polymer and nanotubes. These include extrusion techniques,[12] melt processing,[13] and the use of surfactants to aid dispersion.[14] Many authors have also reported the use of functionalized CNTs to improve the mechanical properties in polymer–CNT composites[15–19]

Another method involves in situ polymerization in the presence of pristine nanotubes. This can result in covalent attachment of nanotubes to the polymer. Consequently, better dispersion and the formation of a strong interface between the nanotubes and the polymer matrix is achieved.[20–25] Using this process with pristine carbon nanotubes, Jia et al.[26] have suggested that during the polymerization, the initiator could open the π bonds of the CNTs and therefore lead to a strong covalent interaction between the nanotubes and the polymer. However, in situ polymerization in the presence of functionalized nanotubes is even more promising owing to the superior dispersion of functionalized nanotubes in solvents and the potential for chemical reactions between the initiator and the functional group. This results in more-complete polymerization and

[*] Dr. J. N. Coleman, D. Blond, Dr. K. P. Ryan, Dr. V. Nicolosi, Prof. W. J. Blau
School of Physics, University of Dublin, Trinity College Dublin
Dublin 2 (Ireland)
E-mail: colemaj@tcd.ie
Dr. V. Barron
National Centre for Biomedical Engineering Science
National University of Ireland
Galway (Ireland)
Dr. M. Ruether
School of Chemistry, University of Dublin, Trinity College Dublin
Dublin 2 (Ireland)

[**] The authors thank Science Foundation Ireland. JNC wishes to thank IRCSET for financial support.

more-effective crosslinking of the polymer with the nanotubes thus increasing the mechanical properties.

In this paper, we have characterized the mechanical properties of composite films fabricated by in situ polymerization of amorphous poly(methyl methacrylate) (PMMA) in the presence of purified chemical vapor deposition (CVD)-produced –OH functionalized multiwalled CNTs (MWNTs) to give a PMMA–CNT blend. Fourier transform infrared (FTIR) spectroscopy studies were carried out that suggest bonding between CNTs and PMMA. A range of composite dispersions with various nanotube mass fractions were formed by blending polymerized PMMA–CNT material with PMMA. Stress–strain measurements were then taken for a range of films fabricated from these dispersions. Mechanical parameters such as the elongation of the composite at break, the Young's modulus, breaking strength, ultimate tensile strength, and toughness all displayed significant increases in the presence of nanotubes.

2. Results and Discussion

It is important to determine whether or not functional groups have been covalently attached to the nanotubes. While Raman spectroscopy can be used for this purpose, it is not ideal, as the main effect of functionalization on the Raman spectrum of the nanotube is an increase in intensity of the disorder (D) band. In the case of CVD-MWNTs the defect density is so high that the D-band is already relatively intense.[27] As such, functionalization is expected to have a minimal effect on the D-band intensity. A much better technique is infrared spectroscopy. Infrared spectroscopy was carried out in the mid-infrared (4000–500 cm^{-1}) region. Spectra were taken for polymerized PMMA and compared with commercial PMMA spectra in order to confirm the integrity of the polymerization reaction. Figure 1 represents the infrared spectrum of CNTs that have reacted with the PMMA during the polymerization (reacted CNTs) compared to unreacted, pristine CNTs.

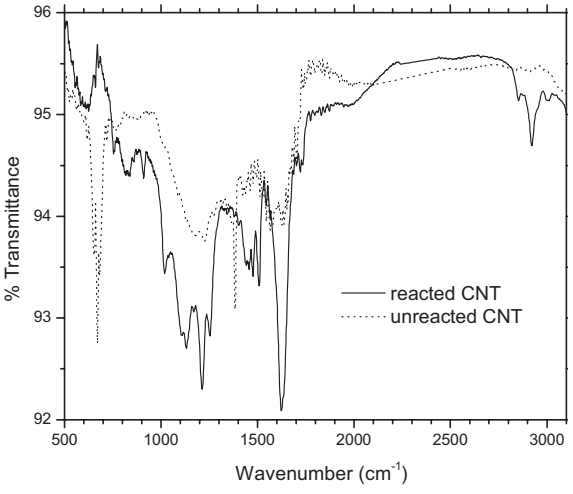

Figure 1. FTIR spectra of reacted and unreacted CNTs.

The reacted spectra were collected after the sample had been washed five times with toluene. In addition, infrared spectroscopy was performed on both pure toluene and each filtrate. While initial filtrates showed evidence of PMMA, the spectra for the final filtrate and toluene were identical, showing that all excess unbounded PMMA had been washed from the nanotubes after five washes. This strongly suggests that any species appearing in the reacted spectra are covalently attached to the nanotubes.

The first three peaks in the reacted spectrum at 3010, 2921, and 2853 cm^{-1} are characteristic of PMMA, and they are not present in the unreacted spectrum. Also, the peak at 1721 cm^{-1} could represent an esteric group present in the PMMA structure. The peak at 1622 cm^{-1} is present only in the reacted spectrum. It corresponds to the C=O vibration of the side chain of PMMA. The intense peak in the unreacted spectrum at 1383 cm^{-1} represents the vibration of alcohol groups (–OH) associated with the original functionality. After the polymerization reaction, this peak was absent from the reacted spectrum, suggesting that bonding occurs between the functionalized groups and the PMMA. The nature of the peak at 681 cm^{-1} is unclear at the present time; however, this peak had completely disappeared in the reacted spectra. As a whole, these FTIR data strongly suggest that at least some of the PMMA chains are covalently attached to the nanotubes. The main peaks observed are summarized in Table 1.

Table 1. IR frequencies of the different compounds of the reacted and unreacted CNTs.

Fragment of reacted CNT	Wavenumber [cm^{-1}]
—CH_2– (acyclic)	2921.19
—O—CH_3 , —CH_2– (acyclic)	2853.25
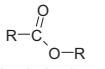	1721.84
C=C, C=O	1622.73
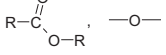	1131.7, 1104.93
—O—	1018.42, 910.33, 838.21
Fragment of unreacted CNT	**Wavenumber (cm^{-1})**
—OH	1383.95

Tensile measurements were carried out in order to determine the mechanical properties of the PMMA composite films. Five measurements on five different strips were performed on each sample for statistical accuracy. Shown in Figure 2 are representative stress–strain curves for some of the composites studied in this work. The strain, ε, represents the fractional elongation while the stress, σ, is the force divided by the cross-sectional area of the unloaded sample.

The pristine polymer displays elastic behavior up to a yield point of $\varepsilon = 0.2\,\%$, followed by a small deformation before fracture occurs at a strain-to-break of $\varepsilon_B = 0.57\,\%$. This low value of strain-to-break is typical for low-molecular-weight polymers such as this material.[28] Dramatic changes in the stress–strain

ADVANCED FUNCTIONAL MATERIALS

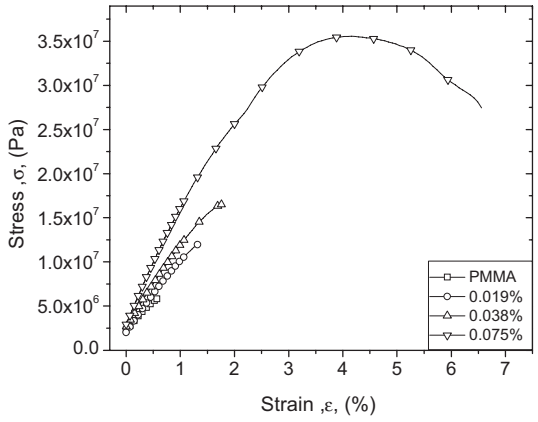

Figure 2. Representative stress–strain curves for PMMA-based composites for a range of nanotubes volume fractions.

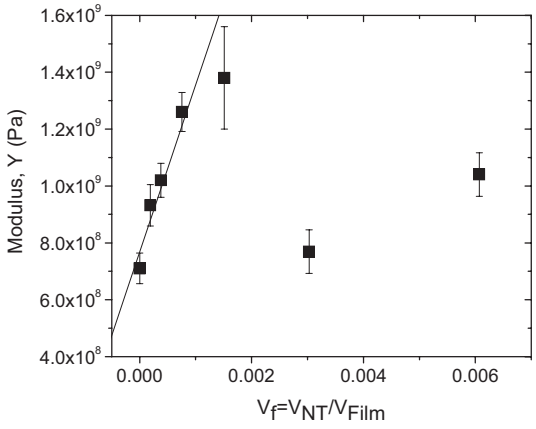

Figure 4. Young's modulus as a function of volume fraction of CNTs.

curves can be observed on the addition of CNTs. As the nanotube content is increased, the yield point increases to approximately $\varepsilon = 0.66$ % for the sample with a volume fraction (V_f) of 0.075 %. In addition, significant plastic deformation is observed for mid-range nanotube-loading levels. The strain-to-break increases steadily with nanotube volume fraction reaching $\varepsilon_B = 6.53$ % for the $V_f = 0.075$ % sample. This is unusual, as most polymer–nanotube composites become brittle on the addition of even small amounts of nanotubes. However, above this volume fraction the strain-to-break does indeed fall off and the material becomes more brittle as more nanotubes are added. This trend is shown in Figure 3.

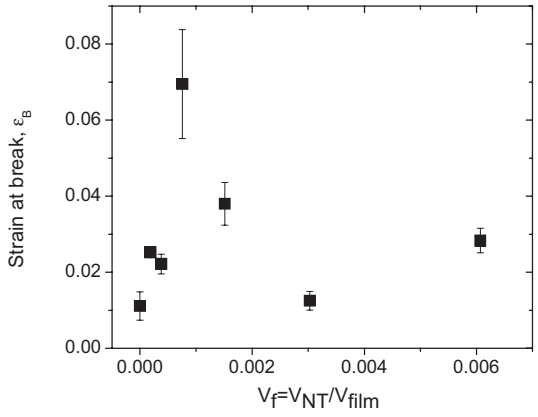

Figure 3. Strain at break as a function of volume fraction of CNTs.

More importantly, for low CNT contents, a remarkable increase in stiffness, strength, and toughness is clearly visible. Shown in Figure 4 are the Young's moduli as a function of V_f of CNTs for all composites studied. Young's modulus (Y) can be defined as the slope of the linear elastic deformation of the stress–strain curve, i.e., $Y = d\sigma/d\varepsilon$ as $\varepsilon \to 0$.

It can clearly be seen from Figure 4 that the Young's modulus increases linearly with volume fraction before falling off at higher volume fractions. This trend is also observed for the other mechanical properties investigated—strength and toughness—and will be discussed below. This linear increase occurs up to an optimum loading level of $V_f = 1.5 \times 10^{-3}$. This represents an increase of ×1.9, from 0.71 GPa to 1.38 GPa. The enhancement of the Young's modulus can be quantified as dY/dV_f, which was found to be 586 ± 89 GPa in this case. This is a useful parameter, as it takes into account the magnitude of the stiffness increase and the nanotube content required to achieve that increase. Moreover, this allows comparison with results in the literature. Previous work[25] preparing PMMA–functionalized-CNT composites by in situ polymerization has shown an increase in the storage modulus of 81 % by adding 0.009 volume fraction of CNTs by thermal mechanical analysis at 40 °C. In this case dY/dV_f was equal to ~146 GPa. A dramatic increase in the storage modulus at 20 °C from 2.5 GPa for pure PMMA to 31 GPa for a composite containing $V_f = 0.13$ PMMA-grafted MWNTs made by emulsion polymerization was also reported.[18] By this method, dY/dV_f was equal to ~203 GPa. In both cases, these results were obtained using dynamic mechanical analysis (DMA). It should be pointed out that the dY/dV_f values presented here are significantly higher than those appearing in the literature for comparable composites. However, due to saturation at relatively low V_f we have not achieved moduli comparable to those discussed by Hwang et al.[18]

Young's modulus data can be analyzed using the rule of mixtures. It describes a simple model to calculate the Young's moduli of carbon-fiber-reinforced polymer composites. In this study, Krenchel's rule of mixtures for short-fiber composites was applied[29]

$$Y_C = (\eta_0 \eta_l Y_{NT} - Y_P) V_f + Y_P \quad (1)$$

where Y_C, Y_{NT}, and Y_P are the composite, nanotube, and polymer moduli, V_f is the nanotube volume fraction, and η_0 and η_1 are efficiency factors related to fiber orientation[29] and length.[30] We assume a preferential orientation of the nanotubes in the plane of the film, in analogy with the situation for PVA–nanotube films.[31] In this case, η_0 can be chosen to be

equal to 3/8.[9,29,31] Previous work based on PVA composites has shown that it is very difficult to separate the contributions of η_1 and Y_{NT}.[9] Therefore, only an effective nanotube modulus defined by

$$Y_{Eff} = \eta_l Y_{NT} \quad (2)$$

can be calculated. An effective nanotube modulus was found to be equal to 1564 ± 140 GPa by using Equations 1 and 2. The effective nanotube modulus is far above the expected modulus values for catalytic nanotubes, which lie in the region of 10 to 500 GPa.[32] It is not clear at this time why such unexpectedly large reinforcement values are occurring in these materials.

The breaking strength, σ_B, and ultimate tensile strength, σ_C, are represented in Figure 5. σ_B corresponds to the stress at which fracture occurs. σ_C represents the maximum stress value applied to the material. In general, for viscoelastic materials there is a clear difference between σ_c and σ_B, with $\sigma_c \geq \sigma_B$.

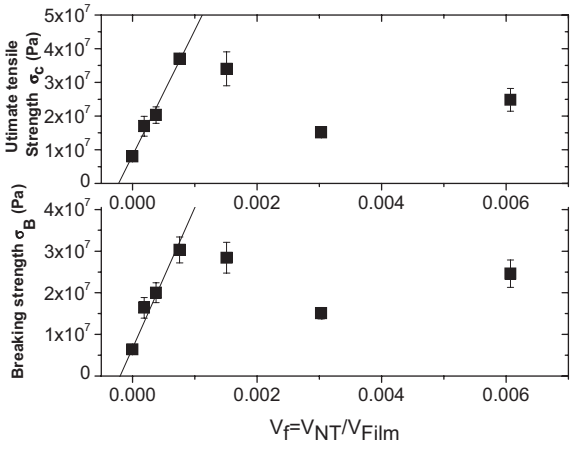

Figure 5. Ultimate tensile strength and breaking strength as a function of volume fraction of CNTs.

However, when the material has a very small plastic deformation, the two parameters can be very similar, or in some cases identical. This is the case for our low-volume-fraction composites, resulting in similar trends for the two parameters.

In both cases a linear increase in strength was observed followed by a fall off. A dramatic increase in σ_C from 8.03 MPa to 37 MPa was observed by adding less than 7.5×10^{-4} V_f of nanotubes. Similarly, an increase in σ_B from 6.4 MPa for the polymer to 30.3 MPa for the 7.5×10^{-4} V_f sample was recorded. The slopes for these linear increases were calculated to be $d\sigma_C/dV_f = 38 \pm 2.4$ and $d\sigma_B/dV_f = 33.7 \pm 3.6$ GPa. It should be pointed out that the low strength of the pure polymer is due to its relatively low molecular weight of 3500 g mol^{-1}, which corresponds to approximately 67 repeat units.

Jia et al.[26] also noticed strength enhancement when using unfunctionalized MWNTs in PMMA composites fabricated by in situ polymerization. Reinforcement of up to 30 % in σ_B was achieved by adding 0.03 volume fraction of CNTs. Velasco-Santos et al.[25] have reported an increase of 75 % in σ_B by using functionalized MWNTs with a volume fraction of $V_f = 0.009$ and a 41 % increase by adding $V_f = 0.006$ unfunctionalized MWNTs.

The strength of fiber-reinforced composites can be described by the rule of mixtures. While this is a simplistic model, we nevertheless feel that it can be used to shed some light on our results. In the framework of this model, if the fibers are longer than the so-called critical length, the rule of mixtures can be expressed by[28]

$$\sigma_B = \left[\left(1 - \frac{l_c}{2l}\right)\sigma_{NT} - \sigma_P\right] V_f + \sigma_P \quad (3)$$

where σ_B, σ_{NT}, and σ_P are the composite, the nanotube, and the polymer strengths, respectively (σ_P is measured from the breaking strength of the polymer, referred to earlier as σ_B). The nanotube length is described by l while l_c represents the critical length. This is the nanotube length below which the polymer can no longer transfer enough stress to break the nanotube. For a hollow cylindrical body, it is given by the expression[33]

$$l_c = \frac{\sigma_{NT} D}{2\tau}\left[1 - \frac{d^2}{D^2}\right] \approx \frac{\sigma_{NT} D}{2\tau} \quad (4)$$

where D is the nanotube outer diameter, d is the diameter of the inner channel, and τ is the interfacial shear strength (IFSS). The approximation is valid for large-diameter nanotubes with narrow inner channels, as we have here. Combining Equations 3 and 4 (neglecting σ_P, which is relatively small), differentiating with respect to V_f, and re-arranging gives a quadratic equation for the nanotube strength. The solution to this equation is:

$$\sigma_{NT} = \tau \frac{2l}{D}\left[1 \pm \sqrt{1 - \frac{D}{\tau l}\frac{d\sigma_B}{dV_f}}\right] \quad (5)$$

The validity of this expression can easily be checked by showing that in the limit where the nanotube length approaches infinity, $\sigma_{NT} \rightarrow d\sigma_B/dV_f$, as expected from Equation 3 (taking the minus sign). For σ_{NT} to be real, the following condition must be imposed

$$\tau \geq \frac{D}{l}\frac{d\sigma_B}{dV_f} \quad (6)$$

Note that this is a harder constraint than the one defining the applicability of Equation 3, i.e., $l \geq l_c$. This is because according to Equation 3, $\sigma_{NT} \geq d\sigma_B/dV_f \geq \sigma_{NT}/2$. Transmission electron microscopy (TEM) studies were carried out to measure the average nanotube diameter and length, resulting in values of $D = 16.6 \pm 3.9$ nm and $l = 1.2 \pm 0.6$ μm. Taking $d\sigma_B/dV_f = 33.7 \pm 3.64$ GPa and applying Equation 6 results in $\tau \geq 470 \pm 400$ MPa. The highest value ever suggested, to the authors' knowledge, is $\tau = 500$ MPa.[34] However it is unlikely that this figure is realistic. Literature values quote that τ should be in the range of 50–100 MPa.[34–38] However, it is more likely

ADVANCED FUNCTIONAL MATERIALS

that τ is close to the value for the polymer shear strength, which is in turn probably close to the polymer tensile strength, $\sigma_P = 6.4$ MPa. Thus we feel that it is unlikely that the inequality expressed in Equation 6 really applies here. This suggests that the average nanotube length is actually less than the critical length in our samples, which means that Equation 3 actually cannot be used here.

The fact that Equation 3 does not apply can be further emphasized by calculating the nanotube strength implied by Equation 5. If we assume Equations 5 and 6 apply in this case then the minimum possible value for the nanotube strength can be found to be $\sigma_{NT} \geq 2d\sigma_B/dV_f$, that is $\sigma_{NT} \geq 67.4 \pm 7.5$ GPa. Given that the highest strength ever recorded for perfectly graphitized nanotubes was $\sigma_{NT} = 63$ GPa,[6] this is unlikely. In fact, owing to their high defect content, catalytic MWNTs such as those used in this work tend to have strengths of the order of a few gigapascals.[39] Thus, it is extremely unlikely that the model described by Equation 3 is appropriate in this case.

An alternative model describes the situation when the nanotube length is less than the critical length. In this case, the nanotubes do not break when a stress is applied to the material. In fact, failure occurs at the polymer/nanotube interface, generally by debonding of the polymer from the nanotube. The following equation represents a tensile-strength model for short-fiber composites under these circumstances:[28]

$$\sigma_B = \left(\frac{l}{2R}\tau - \sigma_P\right)V_f + \sigma_P \tag{7}$$

where σ_P is the polymer breaking strength, and R the radius of the nanotubes. By fitting this equation with the data from Figure 4 we obtained a value for the interfacial stress transfer of 456 ± 378 MPa. This means than the shear strength lies in the range of $78 \leq \tau \leq 834$ MPa. As discussed previously, the interfacial shear strength is expected to lie in the 50–100 MPa range.[34,36–38] Thus, while our calculated τ is within the possible range, it is unlikely that the IFSS is so high, even for covalently functionalized nanotubes. To unambiguously test the applicability of this model, it is necessary to confirm that debonding actually occurs at the polymer/nanotube interface.

In order to test this, scanning electron microscopy (SEM) studies have been carried out on the composites used for mechanical testing. Shown in Figure 6 is an SEM image of a crack in the composite film. A number of 1D objects are observed bridging the crack. While these objects are clearly nanotubes, detailed measurements of their average diameter show it to be much larger than that measured for pristine nanotubes by TEM. The measured average diameter of the objects observed by SEM was 111 nm, which can be compared with the average pristine nanotube diameter of 16 nm. Assuming a thickness for the gold coating of 15 nm, this means the nanotubes are covered with some sort of coating of thickness ca. 33 nm. We suggest that this coating is a very well adhered polymer layer. This layer probably consists of polymer strands that have entangled with the covalently attached functional groups to form a mechanically strong interfacial region. This means that the fracture is unlikely to occur at the polymer/nanotube interface but must occur at the edge of the interfacial region. Therefore, another model is needed. Such a model would take into consideration that the break occurs at a polymer/polymer interface displaced from the polymer/nanotube interface. It can be described by the following equation:[9]

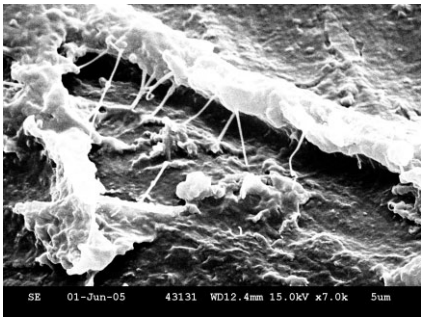

Figure 6. SEM picture of Polymerized PMMA/CNTs Composites.

$$\sigma_B = \left(1 + \frac{b}{R}\right)\left[\frac{l}{2R}\sigma_{Shear} - \left(1 + \frac{b}{R}\right)\sigma_p\right]V_f + \sigma_P \tag{8}$$

where b is the thickness of the polymer coating around the nanotubes and σ_P the breaking strength of the bulk polymer.[9] Here, σ_{shear} is the shear strength of the polymer/polymer interface at the edge of the interfacial region. Applying this model σ_{Shear} was found to be 88 ± 115 MPa, meaning the shear strength is within a range of $0 < \sigma_{shear} \leq 203$ MPa. While the error is very large, the region of uncertainty does in fact encompass the polymer breaking strength, $\sigma_P = 6.4$ MPa. This confirms that this model may, in fact, be the correct one. This means that the covalently attached polymer strands play a dual reinforcement role. They act to increase the polymer/nanotube IFSS as originally expected. However, in addition, they increase the composite strength by entangling with the matrix polymer to create a high-strength interfacial region. This behavior has been observed before for chlorinated polypropylene-functionalized-nanotube composites.[9] In addition, Barber et al. have observed polymer interfacial regions with anomalously high shear strength in pullout measurements.[35] This may explain the high value of σ_{Shear} calculated using Equation 6. One might even speculate that this interfacial region is stiffer than the bulk amorphous polymer. It could then act as an extra component of reinforcement, analogous to the role played by crystalline coatings in poly(vinyl alcohol)-based composites,[9] resulting in higher than expected dY/dV_f values.

The toughness, as shown in Figure 7, is the energy needed to break the composite, and can be calculated from the area under the stress–strain curve. It shows a dramatic linear increase of 1282 % from 0.069 MJ m^{-3} to 0.95 MJ m^{-3} by adding 1.5×10^{-3} V_f of CNTs. The slope, dT/dV_f, was $6.1 \pm 1.38 \times 10^8$ J m^{-3}. In comparison, Jia et al.[26] obtained an increase of 2.7 % by adding 0.03 V_f of treated CNTs and a dT/dV_f value equal to 1281 J m^{-3}. Similarly, an increase of 74.6 % was observed by adding $V_f = 0.009$ of functionalized CNTs.[25]

All mechanical parameters, modulus, strength, and toughness display an approximately linear increase with volume frac-

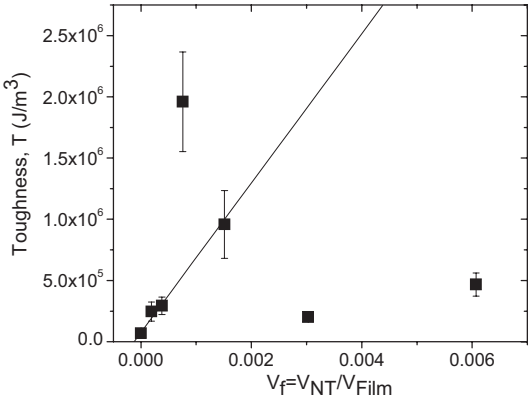

Figure 7. Toughness as a function of volume fraction of CNTs.

tion followed by saturation. This results in an optimal nanotube volume fraction for mechanical reinforcement that is extremely low compared to previous measurements. The decrease in mechanical parameters at higher volume fraction can be explained by nanotube aggregation at higher loading levels, resulting in the formation of stress-concentration centers. This clearly illustrates the importance of good nanotube dispersion at low volume fractions. However, it also shows that the maximum reinforcement is limited by the maximum achievable volume fraction where good dispersion can be maintained. In the future it will be important to try to increase this maximum volume fraction, possibly through careful chemical engineering of the functionalities. All the mechanical results are summarized in Table 2.

3. Conclusions

Polymer composites have been fabricated using PMMA and OH-functionalized MWNTs by in situ polymerization. FTIR studies suggested that bonding between carbon nanotubes and PMMA may occur at the –OH functionality, and also at the outer layer of the CNTs. More analysis needs to be done to confirm these results. Mechanical properties have shown an increase in all the parameters investigated for a low content of carbon nanotubes. These improvements are approximately 94 % for Young's modulus, 360 % for ultimate tensile strength, 373 % for breaking strength, 1282 % for toughness, and 526 % for the elongation at break. The Young's modulus reinforcement, dY/dV_f, shows quite a high value of 586 GPa. Therefore, analysis using Krenchel's rule of mixtures results in a very high value for the effective nanotube modulus, 1564 GPa. Shear stress, τ, was calculated with two different models. The first model gave an unreasonably high value of 456 ± 378 MPa compared to the expected value 50–100 MPa. The second model, which takes into account the microscopy studies, gives the polymer shear strength to be 88 ± 115 MPa. While this is much higher than the expected value of approximately 6.4 MPa it is an acceptable value within the error. Also, the range of the error can be explained by the large variations of length of the nanotubes in the TEM studies. Finally, at higher mass fractions, the mechanical properties tend to fall off. This is probably due to aggregation effects at high concentration.

Table 2. Summary of the main mechanical results.

	dY/dV_f [GPa]	$d\sigma_C/dV_f$ [GPa]	$d\sigma_B/dV_f$ [GPa]	dT/dV_f [J/m^3]	$d\varepsilon_b/dV_f$
Value	586 ± 89	38 ± 2.35	33.7 ± 3.64	(6.1±1.38)×10^8	27.96 ± 10.45
Increase	94%	360%	373%	1282%	526%
	0.71GPa→1.38GPa	8.03MPa→37MPa	6.46MPa→30.3MPa	0.069 MJ/m^3 → 0.95 MJ/m^3	0.011 → 0.0695
Saturation point, (V_f)	1.5 × 10^{-3}	7.5 × 10^{-4}	7.5 × 10^{-4}	1.5 × 10^{-3}	7.5 × 10^{-4}

4. Experimental

PMMA–CNT composites were synthesized using an in situ radical polymerization method. In a typical procedure, MMA monomer (99 %, Aldrich) was distilled twice to remove any impurities. The free-radical initiator azobisisobutyronitrile 2,2 (AIBN, Aldrich) was mixed with 1 g of purified MMA and -OH functionalized thin MWNTs (www.nanocyl.be). The solution was sonicated for 5 min in a sonic bath to remove any trapped air. The quantities of CNTs and AIBN relative to MMA were 1 wt % and 0.25 wt %, respectively. The solution was then stirred and heated to 90 °C for 2 h. Consequently, a homogenous solid PMMA/CNT composite was formed, which was subsequently cured for 12 h at 90 °C. To prepare a range of composite mass fractions, the polymerized sample was dissolved in toluene at a concentration of 30 g L^{-1}. To achieve a good dispersion, the solution was sonicated for 5 min using a high-power sonic tip (120 W, 60 kHz) followed by a mild sonication for 3 h in a sonic bath, followed by further high-power sonication for an additional 5 min. Afterwards, the primary solution was blended with pure PMMA solution polymerized under the same conditions to produce a range of various mass fractions of up to 0.6 vol %. After blending, an extra sonication process was carried out on each sample by using the high-power sonic tip and sonic bath for the same time periods as before. Freestanding films were fabricated by dropping 1 mL of each solution onto a polished Teflon disk that was then placed in an oven at 60 °C to allow the evaporation of the solvent. This procedure was repeated four times in order to obtain an average film thickness of 75 μm. The films were then peeled from the substrate and cut into strips of 10 mm × 2.5 mm × 75 μm. Width and thickness of each strip were measured using a low-torque digital micrometer. For each sample, nanotube mass fractions were converted into volume fraction using the following equation:

$$V_f = \left[1 + \left(\frac{\rho_{NT}}{\rho_{Pol}}\right)\left(\frac{1 - m_f}{m_f}\right)\right]^{-1} \quad (9)$$

where V_f stands for the volume fraction ($V_f = V_{NT}/(V_{NT} + V_P)$) and m_f for the mass fraction ($m_f = m_{NT}/(m_{NT} + m_P)$) of CNTs present in the polymer. ρ_{NT} and ρ_{Pol} are respectively the densities of the CNTs and the polymer matrix. Densities of 2150 kg m^{-3} and 1300 kg m^{-3} were used for nanotubes and polymer respectively [41]. Mechanical testing was performed with a Zwick tensile tester Z100 using a 100 N load cell with a cross-head speed of 0.5 mm min^{-1}. Far-infrared spectrometry was carried out by using a Nicolet FTIR spectrometer. Samples were prepared first by dissolving polymerized PMMA/CNTs in toluene. Then, the solution was washed five times through a filter paper (pore size 0.22 μm) to remove PMMA chains that had not reacted with CNTs. The residue was

then scraped from the filter paper, dried, and mixed with potassium bromide to obtain thin semitransparent films. Raw CNTs were also mixed with KBr for comparative analysis. Gel permeation chromatography (GPC) was carried out to calculate the molecular weight M_w for the polymerized PMMA. An average value for M_w was found to be 3500 g mol^{-1}, which corresponds to approximately 67 repeat units. SEM measurements were performed by using a Hitachi S4300 instruments. To facilitate SEM measurements, samples were first gold coated (15 nm). TEM measurements were made with a Hitachi H-7000 using holey carbon grids (400 mesh).

Received: November 28, 2005
Final version: March 8, 2006
Published online: ■

[1] S. Iijima, *Nature* **1991**, *354*, 56.
[2] B. Q. Wei, R. Vajtai, P. M. Ajayan, *Appl. Phys. Lett.* **2001**, *79*, 1172.
[3] S. Berber, Y. Kwon, D. Tománek, *Phys. Rev. Lett.* **2000**, *84*, 4613.
[4] R. H. Baughman, A. A. Zakhidov, W. A. de Heer, *Science* **2002**, *297*, 787.
[5] E. W. Wong, P. E. Sheehan, C. M. Lieber, *Science* **1997**, *277*, 1971.
[6] M. Yu, O. Lourie, M. J. Dyer, T. F. Kelly, R. S. Ruoff, *Science* **2000**, *287*, 637.
[7] G. G. Tibbetts, C. P. Beetz, *J. Phys. D* **1987**, *20*, 292.
[8] A. B. Dalton, S. Collins, E. Munoz, J. M. Razal, V. H. Ebron, J. P. Ferraris, J. N. Coleman, B. G. Kim, R. H. Baughman, *Nature* **2003**, *423*, 703.
[9] J. N. Coleman, M. Cadek, R. Blake, V. Nicolosi, K. P. Ryan, C. Belton, A. Fonseca, J. B. Nagy, Y. K. Gun'ko, W. J. Blau, *Adv. Funct. Mater.* **2004**, *14*, 791.
[10] M. Cadek, J. N. Coleman, V. Barron, K. Hedicke, W. J. Blau, *Appl. Phys. Lett.* **2002**, *81*, 5123.
[11] S. J. V. Frankland, A. Caglar, D. W. Brenner, M. Griebel, *J. Phys. Chem. B* **2002**, *106*, 3046.
[12] R. E. Gorga, R. E. Cohen, *J. Polym. Sci., Part B: Polym. Chem.* **2004**, *42*, 2690.
[13] R. Haggenmueller, H. H. Gommans, A. G. Rinzler, J. E. Fischer, K. I. Winey, *Chem. Phys. Lett.* **2000**, *330*, 219.
[14] C. Velasco-Santos, A. L. Martinez-Hernandez, F. Fisher, R. Ruoff, V. M. Castano, *J. Phys. D* **2003**, *36*, 1423.
[15] R. Blake, Y. K. Gun'ko, J. Coleman, M. Cadek, A. Fonseca, J. B. Nagy, W. J. Blau, *J. Am. Chem. Soc.* **2004**, *126*, 10226.
[16] C.-C. Hsiao, T. S. Lin, L. Y. Cheng, C.-C. M. Ma, A. C.-M. Yang, *Macromolecules* **2005**, *38*, 4811.
[17] L. Liu, A. H. Barber, S. Nuriel, H. D. Wagner, *Adv. Funct. Mater.* **2005**, *15*, 975.
[18] G. L. Hwang, Y.-T. Shieh, K. C. Hwang, *Adv. Funct. Mater.* **2004**, *14*, 487.
[19] J. Yang, J. Hu, C. Wang, Y. Qin, Z. Guo, *Macromol. Mater. Eng.* **2004**, *289*, 828.
[20] C. Zhao, G. Hu, R. Justice, D. W. Schaefer, S. Zhang, M. Yang, C. C. Han, *Polymer* **2005**, *46*, 5125.
[21] J. Gao, M. E. Itkis, A. Yu, E. Bekyarova, B. Zhao, R. C. Haddon, *J. Am. Chem. Soc.* **2005**, *127*, 3847.
[22] K. W. Putz, C. A. Mitchell, R. Krishnamoorti, P. F. Green, *J. Polym. Sci., Part B: Polym. Chem.* **2004**, *42*, 2286.
[23] S. Kumar, T. D. Dang, F. E. Arnold, A. R. Bhattacharyya, B. G. Min, X. Zhang, R. A. Vaia, C. Park, W. W. Adams, R. H. Hauge, R. E. Smalley, S. Ramesh, P. A. Willis, *Macromolecules* **2002**, *35*, 9039.
[24] C. Park, Z. Ounaies, K. A. Watson, R. E. Crooks, J. Smith, S. E. Lowther, J. W. Connell, E. J. Siochi, J. S. Harrison, T. L. S. Clair, *Chem. Phys. Lett.* **2002**, *364*, 303.
[25] C. Velasco-Santos, A. L. Martinez-Hernandez, F. T. Fisher, R. Ruoff, V. M. Castano, *Chem. Mater.* **2003**, *15*, 4470.
[26] Z. Jia, Z. Wang, C. Xu, J. Liang, B. Wei, D. Wu, S. Zhu, *Mater. Sci. Eng. A* **1999**, *271*, 395.
[27] P. H. Tan, S. L. Zhang, K. T. Yue, F. M. Huang, Z. J. Shi, X. H. Zhou, Z. N. Gu, *J. Raman Spectrosc.* **1997**, *28*, 369.
[28] W. D. Callister, *Materials Science and Engineering, an Introduction*, Wiley, New York **2003**.
[29] H. Krenchel, *Fibre Reinforcement*, Akademisk Forlag, Copenhagen **1964**.
[30] H. L. Cox, *Br. J. Appl. Phys.* **1952**, *3*, 72.
[31] M. S. P. Shaffer, A. H. Windle, *Adv. Mater.* **1999**, *11*, 937.
[32] J. P. Salvetat, A. J. Kulik, J. M. Bonard, G. A. D. Briggs, T. Stockli, K. Metenier, S. Bonnamy, F. Beguin, N. A. Burnham, L. Forro, *Adv. Mater.* **1999**, *11*, 161.
[33] H. D. Wagner, *Chem. Phys. Lett.* **2002**, *361*, 57.
[34] H. D. Wagner, O. Lourie, Y. Feldman, R. Tenne, *Appl. Phys. Lett.* **1998**, *72*, 188.
[35] A. H. Barber, S. R. Cohen, H. D. Wagner, *Appl. Phys. Lett.* **2003**, *82*, 4140.
[36] K. Liao, S. Li, *Appl. Phys. Lett.* **2001**, *79*, 4225.
[37] M. Wong, M. Paramsothy, X. J. Xu, Y. Ren, S. Li, K. Liao, *Polymer* **2003**, *44*, 7757.
[38] C. A. Cooper, S. R. Cohen, A. H. Barber, H. D. Wagner, *Appl. Phys. Lett.* **2002**, *81*, 3873.
[39] S. Xie, W. Li, Z. Pan, B. Chang, L. Sun, *J. Phys. Chem. Solids* **2000**, *61*, 1153.
[40] J. N. Coleman, U. Khan, Y. K. Gun'ko, *Adv. Mater* **2006**, *18*, 689.
[41] D. Qian, E. C. Dickey, R. Andrews, T. Rantell, *Appl. Phys. Lett.* **2000**, *76*, 2868.

Functionalized carbon nanotubes can be used to enhance poly(methyl methacrylate) stiffness, strength, and toughness. However, this reinforcement tends to decrease at volume fractions greater than 0.2% owing to nanotube aggregation. Shown in the figure are polymer-covered nanotubes bridging a crack in a polymer–nanotube composite film.

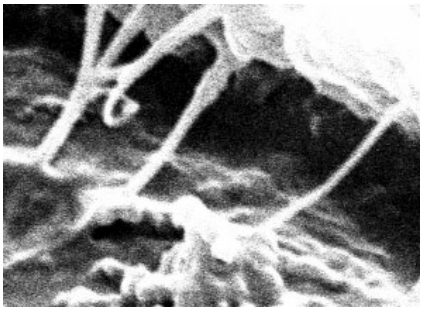

FULL PAPERS

Carbon Nanotube Composites